

Modelling line ratios and continuum SED of NGC4993 and other short GRB host galaxies

M. Contini

School of Physics and Astronomy, Tel Aviv University, Tel Aviv 69978, Israel

5 November 2021

ABSTRACT

We present a detailed spectral modelling of NGC4993 – the host galaxy of GW170817 – and other SGRB host galaxies. In order to determine their physical conditions and the element abundances, we have gathered spectroscopic and photometric data from the literature. The observation data are sometimes missing preventing us from fully constraining the model. However, for most of the SGRB hosts the $[\text{OIII}]5007/\text{H}\beta$ and $[\text{NII}]6548/\text{H}\alpha$ line ratios are reported. The analysis of NGC4993 by a composite model (photoionization+shock) confirms that an AGN, most probably a LINER or a LLAGN, is the gas photoionization source. Shock velocities and preshock densities are similar to those found in the narrow line region of AGN. O/H and N/H have solar values. For the other SGRB of the sample we have found that O/H ratios are nearly solar, while N/H cover a much larger range of values at redshifts close to 0.4. In NGC4993, the relative contribution to the SED of an old stellar population, characterized by a black body temperature of $T_{bb}=4000\text{K}$, with respect to Bremsstrahlung is higher by a factor > 100 than in most of the local AGN and SB galaxies. For the other SGRB composing the sample, T_{bb} ranges between 2000K for SGRB100206A and 8000K for SGRB111117A.

Key words: radiation mechanisms: general — shock waves — ISM: abundances — galaxies: GRB — galaxies: high redshift

1 INTRODUCTION

Gamma-ray bursts (GRB) are short, intense and isolated flashes (Berger 2013), peaking in the gamma-ray band and occurring at an average rate of one event per day over the whole sky (D’Avanzo 2015) with different spectral and temporal properties. The current scenario distinguishes GRBs in “short-hard and long-soft” (Berger 2013) bursts. Short duration GRB (SGRB) last less than 2s, while long GRB (LGRB) have longer duration (Kouveliotou et al 1993). Both the localization and detection of afterglows and hosts and the evidence of lower energy and density scales suggest (Fox et al 2005, Barthelmy et al 2005, Berger et al 2005) that SGRB are cosmological in origin, with low energetic afterglow and that their progenitors are not massive stars (Berger 2013). Berger (2009) claims that the association of some SGRB with elliptical galaxies shows that their progenitors belong to an old stellar population, unlike LGRB. However also SGRB hosts have found to be star forming galaxies. The Swift satellite (Geherls 2004) greatly improved the understanding of SGRB progenitors because revealing their location. At present, the majority of SGRB events appear at relatively low z , at ~ 0.4 - 0.5 on average (Berger 2014).

This is an important issue because it could be related to the nucleosynthesis evolution of the host galaxy stars (Contini 2017a). The lack of an associated supernova in SGRB and the heterogeneous sample of host galaxies (e.g. Kann et al. 2011) is consistent with a compact binary merger origin (Rosswog et al. 2003), such as neutron stars or black holes. The progenitors were related to an old star population compatible with NS (neutron star) -NS or NS-BH (black hole) encounters (Berger 2009, Eichler et al 1989). The host galaxy analysis shows that long GRB are found in star-forming galaxies (Fruchter et al 2006, Savaglio et al 2009 etc) while SGRB occur in both star-forming and early-type galaxies (D’Avanzo et al 2015, Bloom et al 2002, Berger et al 2005, Fox et al 2005, Savaglio et al 2009, Fong et al 2013). SFR in SGRB hosts are low and a broad range of stellar masses is found in agreement with an old progenitor adapted to the merging neutron stars (Perley et al 2012). The discovery of GW170817 the neutron star merger directly measured in gravitational waves and associated with a SGRB allows to study neutron star mergers in general and to investigate, in particular, whether the gas within the

NGC4993 host galaxy has peculiar characteristics (Levan et al 2017, Villar et al 2017, etc).

In previous papers (e.g. Contini 2016) we have been investigating the physical conditions and the element abundances of GRB host galaxies by the analysis of the observed line spectra at relatively high z . We have compared them with those of various supernova (SN) types, active galactic nuclei (AGN), starbursts (SB), HII regions, etc. In this paper we investigate line ratios and continuum SED of SGRB host galaxies. The modelling of the continuum is less constraining than that of the line spectra, so we chose in our sample SGRB hosts that have reported emission line fluxes. The sample is rather poor in number of objects. The line spectra suitable to constrain the models generally contain at least [OII], [OIII], $H\beta$, $H\alpha$ and [NII]. The $H\alpha/H\beta$ line ratios which are used to reddening correct the spectra cannot be neglected.

In our model we assume that the continuum radiation, in terms of thermal Bremsstrahlung, originates from the same clouds of gas emitting the line fluxes. Besides the effect of merging that affects both high redshift galaxies as well as local ones, shock waves are created by winds, jets and collisions throughout the galaxies. Therefore shocks should be accounted for by the calculation of line and continuum fluxes. In particular, shocks with velocities $> 300 \text{ km s}^{-1}$ can heat the gas to high temperatures $> 10^6 \text{ K}$ which decrease following the cooling rate downstream. Consequently, the calculated Bremsstrahlung covers the entire frequency range from radio to X-rays. The flux from the background old star population emerges from the Bremsstrahlung SED in the IR range in local and high z galaxies (Contini 2018). Therefore, in order to reproduce the observed SED we consider that Bremsstrahlung could dominate throughout some significant frequency domains such as the radio, the optical-UV and the soft X-ray, while dust reprocessed radiation appears in the far-IR. Furthermore, synchrotron radiation created by the Fermi mechanism at the shock front is often observed in the radio range.

NGC4993 has enough published data to allow line and continuum modelling. For all other SGRB hosts presented in this paper, the continuum SED observations cover only the IR range corresponding to emission from the underlying stellar population. However, for GRB050709, GRB100206A, GRB130603B the data for the optical-near IR line ratios reported by Berger (2009), Perley et al (2012), de Ugarte Postigo et al (2014), Cucchiara et al (2013) and Soderberg et al (2006) are enough to constrain the models. The code SUMA calculates the continuum as well as the line fluxes. We will show the continuum SED in the diagrams throughout a large frequency range (10^8 - 10^{19} Hz) even if we could find no data in the radio, far-IR, optical-UV and X-ray. The Bremsstrahlung results are presented as predictions. For GRB111117A at $z=2.21$ no line fluxes are reported in the literature. So we will investigate only the old star contribution to the SED in order to compare it to the SED of other SGRB hosts at lower z .

The calculation code SUMA is presented in Sect. 2. In Sect. 3 we report the detailed modelling of line and continuum spectra for each of the SGRB host sample. Concluding remarks follow in Sect. 4.

2 DESCRIPTION OF THE CALCULATIONS

The code SUMA simulates the physical conditions of an emitting gaseous cloud under the coupled effect of photoionization from a radiation source and shocks assuming a plane-parallel geometry (Ferland et al 1995). Two cases are considered relative to the cloud propagation : the photoionizing radiation reaches the gas on the cloud edge corresponding to the shock front (infalling) or on the edge opposite to the shock front (ejection).

To calculate the line flux and the continuum emitted from a gas the physical conditions and the fractional abundances of the ions must be known. In a shock dominated regime the calculations start at the shock front where the gas is compressed and thermalized adiabatically, reaching the maximum temperature ($T \propto V_s^2$, where V_s is the shock velocity) in the immediate post-shock region. Compression is calculated by the Rankine-Hugoniot equations (Cox 1972) for the conservation of mass, momentum and energy throughout the shock front and downstream. Compression strongly affects the cooling rate and consequently, the distribution of the physical conditions downstream, as well as that of the element fractional abundances. The downstream region is automatically cut in many plane-parallel slabs (up to 300) with different geometrical widths in order to account for the temperature gradient throughout the gas. Thus, the change of the physical conditions downstream from one slab to the next is minimal. In each slab the fractional abundances of all the ions is calculated resolving the ionization equations which account for the ionization mechanisms (photoionization by the primary and diffuse radiation and collisional ionization) and recombination mechanisms (radiative, dielectronic recombinations) as well as charge transfer effects. The ionization equations are coupled to the energy equation (Cox 1972), when collisional processes dominate, and to the thermal balance equation if radiative processes dominate. This latter balances the heating of the gas due to the primary and diffuse radiations reaching the slab and the cooling due to recombinations and collisional excitation of the ions followed by line emission and thermal Bremsstrahlung. The coupled equations are solved for each slab, providing the physical conditions necessary to calculate the slab optical depth and the line and continuum emissions. The slab contributions are integrated throughout the nebula. The calculations stop when the electron temperature is as low as 200 K, if the nebula is radiation-bounded or at a given value of the nebula geometrical thickness, if it is matter-bounded. The uncertainties of the calculation results are evaluated as < 10 percent.

The main input parameters are those referring to the shock, which are the preshock density n_0 , the shock velocity V_s , the magnetic field B_0 (for all galaxy models $B_0=10^{-4}$ Gauss is adopted), as well as those characterizing the source ionizing radiation spectrum, and the chemical abundances of He, C, N, O, Ne, Mg, Si, S, Ar, Cl and Fe, relative to H. Generally, V_s is constrained by the FWHM of the line profiles, n_0 by the ratio of the characteristic lines. The relative abundances of the elements are constrained by the line ratios. In the case where shock and photoionization act on opposite sides of a plan-parallel nebula, the geometrical width of the nebula, D , is an input parameter. The diffuse radiation bridges the two sides, and the smaller D

the more entangled are the photoionized and the shocked regions on the opposite sides of the nebula. In this case, a few iterations are necessary to obtain the physical conditions downstream. The effect of dust present in the gas, characterized by the dust-to-gas ratio d/g and the initial grain radius a_{gr} are also consistently taken into account.

The main characteristics of SUMA are explained in detail in the following sections.

2.1 Photoionizing radiation flux

The radiation from a photoionizing source is characterized by its spectrum, which is calculated at 440 energies, from a few eV to KeV, depending on the object studied. Due to radiative transfer, the radiation spectrum changes throughout the downstream slabs, each of them contributing to the optical depth. The calculations assume a steady state downstream. In addition to the radiation from the primary source, the effect of the diffuse secondary radiation created by the gas emission (line and continuum) is also taken into account (see, for instance, Williams 1967), using about 240 energies to calculate the spectrum. The secondary diffuse radiation is emitted from the slabs of gas heated by the radiation flux reaching the gas and by the shock. Primary and secondary radiation are calculated by radiation transfer.

For an AGN, the primary radiation is the power-law radiation flux from the active centre F in number of photons $\text{cm}^{-2} \text{s}^{-1} \text{eV}^{-1}$ at the Lyman limit and spectral indices $\alpha_{UV} = -1.5$ and $\alpha_X = -0.7$. F is combined with the ionization parameter U by $U = (F/(nc(\alpha - 1)))((E_H)^{-\alpha+1} - (E_C)^{-\alpha+1})$ (Contini & Aldrovandi, 1983), where E_H is H ionization potential and E_C is the high energy cutoff, n the density, α the spectral index, and c the speed of light.

If the stars are the photoionization source the number of ionizing photons $\text{cm}^{-2} \text{s}^{-1}$ produced by the hot source is $N = \int_{\nu_0} B_\nu / h\nu d\nu$, where $\nu_0 = 3.29 \times 10^{15} \text{s}^{-1}$ and B_ν is the Planck function. The flux from the star is combined with U and n by $N (r/R)^2 = Unc$, where r is the radius of the hot source (the stars), R is the radius of the nebula (in terms of the distance from the stars), n is the density of the nebula and c is the speed of light. Therefore, T_* and U compensate each other, but only in a qualitative way, because T_* determines the frequency distribution of the primary flux, while U represents the number of photons per number of electrons reaching the nebula. The choice of T_* and U is obtained by the fit of the line ratios.

In the turbulent regime created throughout a SB shocks are ubiquitous. Radiation from the stars photoionizes the gas. For SBs we assume for the primary radiation a blackbody (bb) corresponding to an effective temperature T_* and a ionization parameter U . A pure bb radiation accounting for T_* is a poor approximation for a SB, even adopting a dominant spectral type (see Rigby & Rieke 2004). Following Rigby & Rieke, "the starburst enriches and heats its ISM as well as the intergalactic medium. The ionizing spectrum is set by the SB age, IMF and star formation history." Adopting a single effective temperature the entire SB field is represented by a single star type. However, the observed line spectra for high redshift galaxies at present cover a narrow optical-near-IR range of frequencies, the lines are few and from few ionization levels, therefore the bb radiation flux

calculated by a dominant temperature is acceptable, also in view that the line ratios (that are related to T_*) in a shock dominated regime also depend on the electron temperature, density, ionization parameter, metallicity, on the morphology of the ionized clouds, and in particular, they depend on the hydrodynamical field. Therefore we will determine T_* phenomenologically by selecting the effective temperature T_* which leads to the best fit of all the observed line ratios for each spectrum and we will use it to calculate the continuum.

2.2 Electron temperatures

The temperature in each slab depends on energy gains (G) and losses (L) of the gas. Close to the shock front downstream, collisional mechanisms prevail and the temperature is calculated from the energy equation in terms of the enthalpy change (Cox 1972). In the slabs where the temperature is $\leq 2 \times 10^4$ K, photoionization and heating by both the primary and the secondary radiation dominate and the temperature is calculated by thermal balance ($G=L$). Gains are calculated by the rate at which energy is given to the electrons by the radiation field (Osterbrock 1974). The energy of suprathermal electrons created by photoionization is rapidly distributed among the thermal electrons through collisions, heating the gas.

Several processes contribute to the gas cooling. The cooling rate is: $L = L_{ff} + L_{fb} + L_{lines} + L_{dust}$, where L_{ff} corresponds to Bremsstrahlung, particularly strong at high temperatures and high frequencies. Self-absorption is included in the calculations. L_{fb} corresponds to free-bound losses due to recombination and is high at $T \leq 10^5$ K. L_{lines} is due to line emission with the bulge between $\leq 10^4$ K and 10^5 K. L_{dust} represents the energy lost by the gas in the collisional heating of dust grains. It is high the higher d/g and a_{gr} .

Immediately behind the shock front the gas is thermalized to a temperature of $T = 1.5 \times 10^5 (V_s / (100 \text{ km s}^{-1}))^2$ K. At high temperatures ($\geq 10^6$ K) recombination coefficients are very low. The cooling rate is then low. Considering that the cooling rate is $\propto n^2$ (where n is the density of the gas), the thickness of the first slab depends strongly on n .

At T between 10^4 K and 10^5 K the UV lines and the coronal lines in the IR are strong and lead to rapid cooling and compression of the gas. If the cooling rate is so high to drastically reduce the temperature eluding intermediate ionization-level lines, the calculated spectrum will be wrong. Therefore, the slab thickness must be reduced and all the physical quantities recalculated. The choice of the slab thickness is determined by the gradient of the temperature. This process is iterated until the thickness of the slab is such as to lead to an acceptable gradient of the temperature $(T(i-1) - T(i))/T(i-1) \leq 0.1$, where $T(i)$ is the temperature of slab i .)

As the temperature drops, a large region of gas with temperature $\sim 10^4$ K, which is sustained by the secondary radiation, is present in the radiation-bounded case, i.e. when the gas recombines completely before reaching the edge of the nebula opposite to the shock front. Due to a lower temperature gradient, calculations in this zone may be performed in slabs with a larger geometrical thickness.

2.3 Element abundances

The absolute line fluxes for the ionization level i of element K are calculated by the term $n_K(i)$ which represents the density of the ion i . We consider that $n_K(i) = X(i)[K/H]n_H$, where $X(i)$ is the fractional abundance of the ion i calculated by the ionization equations, $[K/H]$ is the relative abundance of the element K to H and n_H is the density of H (by number cm^{-3}). In models including shock, n_H is calculated by the compression equation (Cox 1972) in each slab downstream. So the abundances of the elements are given relative to H as input parameters.

2.4 Dust reprocessed radiation

Dust grains are coupled to the gas across the shock front by the magnetic field (Viegas & Contini 1994). They are heated by radiation and collisionally by the gas to a maximum temperature which is a function of the shock velocity, of the chemical composition and of the radius of the grains, up to the evaporation temperature ($T_{\text{dust}} \geq 1500$ K). The grain radius distribution downstream is determined by sputtering, which depends on the shock velocity and on the density. Throughout shock fronts and downstream, the grains might be destroyed by sputtering. The grains are heated by the primary and secondary radiation, and by gas collisional processes. Details of the calculations of the dust temperature are given by Viegas & Contini (1994). When the dust-to-gas ratio d/g is high, the mutual heating of dust and gas may accelerate the cooling rate of the gas, changing the line and continuum spectra emitted from the gas. The intensity of dust reprocessed radiation in the IR depends on d/g and on the radius a_{gr} . In this work we use $d/g = 10^{-14}$ by number for all the models which corresponds to 4.1×10^{-4} by mass for silicates (Draine & Lee 1994).

3 MODELLING HOST GALAXY SPECTRA

The spectra observed from SGRB hosts are often poor in number of lines. BTP diagrams (Kauffmann 2003, Kewley et al 2001) for the $[\text{OIII}]/5007/\text{H}\beta$ and $[\text{NII}]/6583/\text{H}\alpha$ line ratios are generally adopted by the author community in order to identify the galaxy type in terms of the radiation source. However, extreme physical conditions and relative abundances far from solar, in particular for O/H and N/H , may shift the observed $[\text{OIII}]/\text{H}\beta$ and $[\text{NII}]/\text{H}\alpha$ line ratios throughout the BTP diagram towards sectors which were assigned to different galaxy types. For example, a low N/H relative abundance may shift the observed $[\text{NII}]/\text{H}\alpha$ line ratio emitted from a galaxy towards the SB galaxy domain although other features of the same object are characteristic of an AGN. This may occur to GRB host galaxies which are located at redshifts higher than local. At high z , over- and under-abundances of the heavy elements are an important issue linked with merging, ages and evolution. So, to constrain a model when the line ratios are few we follow a different method. $[\text{OIII}]/5007/\text{H}\beta$ and $[\text{NII}]/6548/\text{H}\alpha$ data are generally observed because $\text{H}\beta$, $\text{H}\alpha$, $[\text{OIII}]$, $[\text{OII}]$ and $[\text{NII}]$ are the strongest lines in the optical range. A first hint to the choice of the model is obtained by comparing

the observed line ratios with the grids of composite models (photoionization+shock) previously calculated (e.g. Contini & Viegas 2001a,b, hereafter CV01a and CV01b). These models provide an approximated but rich information of the gas physical conditions calculated within the emitting clouds. (The line and continuum radiation flux are calculated at the nebula). The line ratios presented by the grids are adapted to HII regions and AGN, respectively. The models (CV01a) corresponding to a black body photoionization flux can be applied to SB galaxies (see Sect. 2). The $[\text{OIII}]/\text{H}\beta$ and $[\text{NII}]/\text{H}\alpha$ line ratios alone cannot definitively constrain the model because we deal with two line ratios related to two different elements. $[\text{OIII}]/\text{H}\beta$ ratios depend mostly on the ionization parameter and on V_s but the $[\text{NII}]/\text{H}\alpha$ ratios depend strongly on the N/H relative abundances. For e.g. SN and GRB hosts N/H ranges between ~ 0.1 solar and ~ 5 solar (Contini 2017a). We cannot determine a priori whether the best fit to the observed $[\text{NII}]/\text{H}\alpha$ line ratio could be reached by changing one or more input parameters representing the physical conditions (V_s , n_0 , D , F for AGN, T_* and U for SB) or by modifying the N/H relative abundance. N^+ and H^+ ions as well as O^+ and H^+ are correlated by charge exchange reactions, therefore they have a similar trend throughout a cloud. When $[\text{OIII}]/\text{H}\beta$ (and $[\text{OII}]/\text{H}\beta$) are well reproduced by modelling and solar N/H are adopted, the resulting N/H is calculated by $([\text{NII}]/\text{H}\beta)_{\text{obs}} = ([\text{NII}]/\text{H}\beta)_{\text{calc}} (\text{N}/\text{H})/(\text{N}/\text{H})_{\odot}$, where $(\text{N}/\text{H})_{\odot}$ is the solar N/H relative abundance. $[\text{OII}]/\text{H}\beta$ and $[\text{OIII}]/\text{H}\beta$ are more affected by the physical conditions of the emitting gas than by O/H .

On this basis we calculate a grid of models. A set of models (e.g. Table 1) which best reproduce the line ratios is selected. We obtain the final model by comparing the calculated SED with the observed one.

The calculated continuum SED is represented in the diagrams by two lines, one for the Bremsstrahlung which covers frequencies from radio to X-ray, and one for the reprocessed radiation from dust in the IR range. They are calculated by the same model which reproduces the line ratios. In the IR-optical range the background star flux emerges from Bremsstrahlung and can be blended with dust reradiation when shock velocities are high. The errors in the observed photometric data are < 20 percent while the uncertainties in the calculations are < 10 percent.

In Sect. 3.1 we reproduce by detailed modelling the NGC4993 observed line ratios and the continuum SED (Levan et al 2017, Palmese et al. 2017, Wu et al 2017). In Sect. 3.2 we present modelling results of the line spectra observed from the host galaxies included in the Berger (2009) SGRB sample. The calculated continuum is compared to the SED observed by Savaglio et al (2009) in the IR for SGRB050709. In Sect. 3.3 we show the modelling of line and continuum spectra reported by Perley et al (2012) for SGRB100206A host. In Sect. 3.4 the line ratios observed from the SGRB130603B (de Ugarte Postigo et al 2014) and SGRB051221a (Soderberg et al 2006) host galaxies and modelled by Contini (2016) are reported. SGRB130603B has been observed in the IR allowing the modelling of the SED. In Sect. 3.5 the modelling of the SGRB111117A continuum observed by Selsing et al (2017) in the IR is shown.

Table 1. Modelling NGC4993 observed line ratios $[\text{OIII}]/\text{H}\beta=1.4$ and $[\text{NII}]/\text{H}\alpha=1.26$

mod	$[\text{OIII}]/\text{H}\beta$	$[\text{NII}]/\text{H}\alpha$	$\text{H}\beta$ 1	V_s km s^{-1}	n_0 cm^{-3}	D pc	T_* 10^4K	U	$\log F$ 2	$12+\log(\text{O}/\text{H})$	$12+\log(\text{N}/\text{H})$
modSB	1.41	0.13	37.7	300	300	1.67	5	1	-	8.82	8.0
modSD	1.4	0.146	0.0009	100	100	1.9	-	-	-	8.82	8.0
modAGN1	1.43	1.26	0.05	100	300	1	-	-	9.55	8.82	8.0
modAGN2	1.45	0.11	16.9	300	300	0.27	-	-	9.48	8.82	8.0

¹ in $\text{erg cm}^{-2} \text{s}^{-1}$ calculated at the nebula; ² in $\text{photons cm}^{-1} \text{s}^{-1} \text{eV}^{-1}$ at the Lyman limit

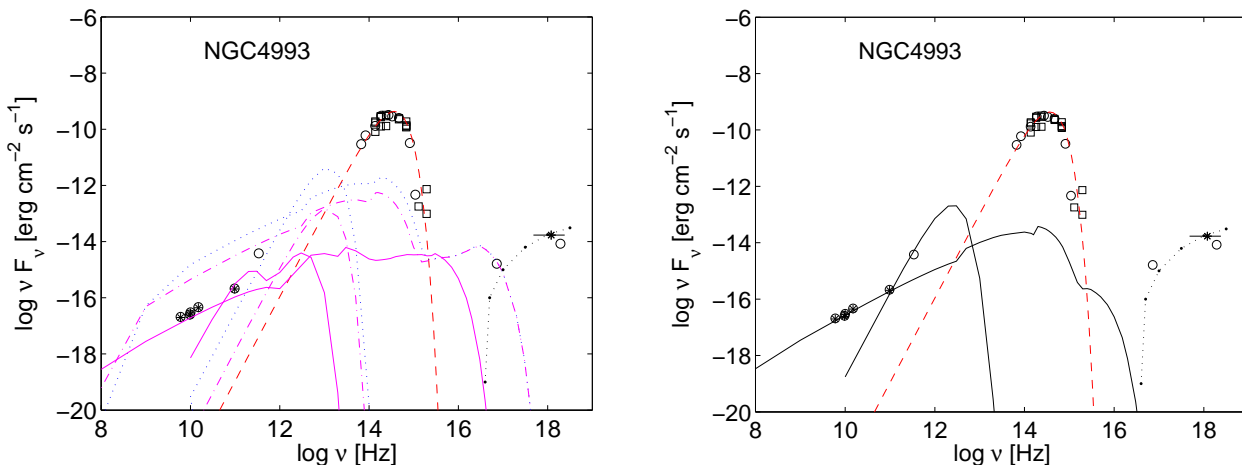


Figure 1. NGC4993 SED data : Wu et al (open circles); Levan et al (open squares); Blanchard et al IR-optical (asterisks); AGN (from NGC5252) flux in the X-rays (dots). bb flux corresponding to 4000 K (red dashed). Left : models modAGN2 (magenta dot-dashed), modSB (blue dotted) and modSD (magenta solid) Right : model modAGN1 (black solid line) ; other symbols as in Fig. 1 left diagram. The models are described in Table 1.

3.1 NGC4993 : the host galaxy of GW170817

Observations by Ligo and Virgo reported gravitational waves which followed to the recent neutron star merger event GW170817. In the frame of our analysis of GRB host line and continuum SED we calculate the characteristics of the emitting gas from NGC4993 which is considered to be the host galaxy of GW170817 at $z=0.009873$.

Levan et al (2017) in their fig. 4 compared $[\text{OIII}]/\text{H}\beta$ and $[\text{NII}]/\text{H}\alpha$ spectroscopic observations with BTP diagnostics. They found that the line ratios fitted the AGN domain. Spectroscopic observations by Palmese et al (2017, fig. 3 right panel) show $[\text{OIII}]5007/\text{H}\beta$ and $[\text{OII}]/\text{H}\alpha$ within the error of Levan et al (2017) observations. However, Palmese et al admitted that the $[\text{OIII}]/\text{H}\beta$ line ratio is very uncertain. In Table 1 we report the calculated models which best reproduce Levan et al spectroscopic data. For all of them O/H solar (6.6×10^{-4}) and N/H solar (10^{-4}) are adopted (Grevesse & Sauval 1998). Model modSB is characterised by a bb photoionizing radiation (suitable to SB and HII regions) and relatively high shock velocities ($V_s = 300 \text{ km s}^{-1}$), modSD is a shock dominated model ($F=0$ and $U=0$) with $V_s = 100 \text{ km s}^{-1}$. Models modAGN1 and modAGN2 are calculated by a power-law photoionizing flux and different shock velocities $V_s = 100 \text{ km s}^{-1}$ and $V_s = 300 \text{ km s}^{-1}$, respectively.

Wu et al (2017) present new Very Large Array (VLA) and ALMA data and use them for broad band modelling.

The continuum SED is shown in Fig. 1. Haggard et al (2017) report Chandra observations which reveal a compact source consistent with the nucleus of the galaxy and $L_X \sim 2 \times 10^{39} \text{ erg s}^{-1}$ (0.5-8 keV). Wu et al suggest that the X-ray soft energy excess may indicate thermal emission from a gaseous component in the galaxy. Some observations in the IR were also available (Lambert & Valentijn 1989, DeVaucouleurs et al 1991, 2MASS 2003). They are used to constrain the model.

In Figs. 1-4 accounting for the continuum SED, each model corresponds to two curves (Bremsstrahlung and dust reradiation). The same symbol is used for both. The models which reproduce the SED in Fig. 1 are those used to fit the line ratios in Table 1. Shock velocities $V_s = 300 \text{ km s}^{-1}$ which correspond to a maximum temperature downstream $T \sim 10^6 \text{ K}$ shift the Bremsstrahlung maximum to relatively high frequencies and fit the datum at $7.25 \times 10^{17} \text{ Hz}$ (Fig. 1, left diagram), corresponding to soft X-ray. However, the continuum SED in the radio-FIR range calculated by models modSB and modAGN2 overpredicts the data in the radio range by a factor of ~ 10 . So we dropped modSB and modAGN2. The shock dominated model (modSD) calculated with $V_s = 100 \text{ km s}^{-1}$ and $n_0 = 100 \text{ cm}^{-3}$ could fit the radio-FIR data adopting a low $d/g = 4 \times 10^{-5}$. In this case the data in the X-ray have no valid explanation. Moreover, the $[\text{NII}]/\text{H}\alpha$ ratio is underpredicted by a factor of 10. To adopt N/H relative abundance 10 times solar in order to fit the $[\text{NII}]/\text{H}\alpha$ ratio is rather an extreme solution. Therefore

we select modAGN1 as the best reproducing model regarding both the line ratios and the SED of NGC4993. The model is calculated with $V_s = 100 \text{ km s}^{-1}$ and $n_0 = 300 \text{ cm}^{-3}$. These shock velocities and densities are found in the narrow line region (NLR) of AGN. The power-law flux is relatively low, suitable to low-luminosity AGN (LLAGN, e.g. Contini 2004) and LINERs.

As already mentioned we calculate the continuum at the nebula whereas the data are observed at Earth. The same is valid for the $H\beta$ line flux. To reduce the calculated $H\beta$ flux by the distance galaxy - Earth, we combine the $H\beta$ flux observed at Earth with $H\beta$ calculated at the nebula by :

$H\beta_{calc} \times r^2 \times ff = H\beta_{obs} \times d^2$. $H\beta_{calc}$ is given in Table 1. $H\beta_{obs}$ is obtained from the Kennicutt (1998) relation linking SFR with $H\alpha$, adopting $H\alpha/H\beta=3$ and $SFR = 0.003 M_\odot \text{ yr}^{-1}$ (Pan et al 2017). ff is the filling factor, r the distance of the nebula from the radiation source and d the distance of the galaxy to Earth. We obtain the factor $f_s = (r/d)^2 = H\beta_{obs} / H\beta_{calc} / ff$ which we use in Fig. 1 to shift the calculated continuum SED in order to be compared with the data observed at Earth. In fact we consider that the Bremsstrahlung is emitted from the same cloud which emits the lines (e.g. $H\beta$). From Fig. 1 (right diagram) the best fit in the radio-NIR range is obtained by $\log(f_s) = -11.7$, while $\log(H\beta_{obs}/H\beta_{calc}) = -14$. Then we obtain $ff=0.005$. The distance from Earth $d=42.9 \text{ Mpc}$, then r results 60 pc . To reproduce the dust reradiation bump in Fig. 1 (right) we adopted $d/g=0.008$ and $a_{gr}=0.1 \mu\text{m}$.

Considering that an AGN is present in the NGC4993 galaxy, we try to fit the X-ray data presented by Wu et al by the (absorbed) power-law model which was successfully adopted to reproduce the X-ray at high frequencies observed for other AGN e.g. the Circinus galaxy (Contini, Prieto & Viegas 1998a), NGC5252 (Contini, Prieto & Viegas 1998b), etc. The observed X-ray flux from the NGC4993 AGN nucleus is relatively low, exceeding the maximum radio flux by a factor of ~ 100 (Fig. 1 right), while in e.g. the Circinus AGN this factor is $> 10^5$ and in NGC5252 ≥ 1000 . Wu et al claim that this X-ray emission is mostly due to a weak LLAGN. The results agree with Palmese et al (2017) who believe that the stellar model fit to NGC4993 reveals the existence of weak ionized gas emission while the line ratios are most probably produced by a harder ionizing source than star formation because lying in the AGN region of the Baldwin et al (1981) diagram. Blanchard et al (2017) argue that there is a weak AGN present in the core of the galaxy on the basis of radio and X-ray emission in agreement with Wu et al (2017) who suggest a LLAGN or even some sort of shocks. Palmese et al concluded that there is no evidence of recent star-formation from the spectrum, irrespective of the uncertain $[OIII]/H\beta$. From the Balmer decrement they found $E(B-V)=0.12 \pm 0.50$. Dust obscuration does not play a role in SFR estimation calculated on the basis of the $H\alpha$ luminosity.

Summarising, the observed SED presented by Wu et al shows soft and hard X-ray emission at $\log(\nu[\text{Herz}]) \geq 17.8$. Our modelling confirms that velocities throughout NGC4993 are $\sim 100 \text{ km s}^{-1}$. Therefore, both soft and hard X-rays (Fig. 1, left diagram) come from the AGN radiation. On the other hand, comparison with the SED calculated with $V_s \geq 300 \text{ km s}^{-1}$ could nicely fit NGC4993 data in the soft X-rays domain. But this model is dismissed because over-

predicting the data in the radio range. Moreover, it corresponds to $[NII]/H\alpha=0.16$. Fig. 1 shows that bb radiation flux from the background population stars corresponding to $T_{bb}=4000\text{K}$ is high relative to Bremsstrahlung.

Concluding with Palmese et al., NGC4993 experienced a minor galaxy merger with still visible signs. The spectral analysis shows AGN activity and an old stellar population. In the IR-optical domain the bb radiation corresponding to the old star background population at 4000 K reproduces the data satisfactorily. Compared to local SB and AGN galaxies (Contini & Contini 2007), the bb flux-to-Bremsstrahlung ratio of > 100 for old stars in the IR-VIS frequency range is remarkably high.

3.2 Berger (2009) sample

The Berger sample of SGRB hosts is relatively poor in number of objects. In Table 2 we present the observed SGRB host galaxy line fluxes. The observed line ratios to $H\beta$ (in the underlying row) for each object are followed in the next row by the calculated ones. The models, represented by the set of the main input parameters which leads to the best fit, are shown in Table 3. In the last column of Table 3 the metallicities evaluated by Berger (2009) are shown. The lines are observed at Earth but calculated at the emitting nebula. We compare the calculated line ratios to the observed line ratios to $H\beta$ corrected for reddening. For SGRB061006 and SGRB070724 $H\alpha$ and $[NII]$ are lacking and the line ratios to $H\beta$ are modelled directly without reddening correction. The $[OII] 3727+$ doublet which is close to the near UV domain is more affected by correction than the other observed lines in the optical-IR. Nevertheless, the ensemble of the parameters which represents the model should be taken with caution. GRB51221a will be shown in Sect. 3.4. Berger (2009) analysing the spectra by the strong line methods, found that short GRB host luminosities are systematically brighter than those of long GRB in the same redshift range. Berger obtained luminosities $L_B \sim 0.1-1.5 L_\odot$, $SFR \sim 0.2-6 M_\odot \text{ yr}^{-1}$ and metallicities $12+\log(O/H) \sim 8.5-8.9$ (3.2×10^{-4} and 7.9×10^{-4} , respectively) higher than for LGRBs. Specific SFR for SGRB have a median value lower than for LGRB SFR hosts. Comparing the results obtained for the Niino et al (2016) sample of LGRB hosts (Contini 2017b) to the present ones in Tables 3 and 5, we obtain similar results.

We have selected SGRB050709 and SGRB050724 photometric data from the Savaglio et al (2009) sample to model the SED. They show at least 3 datapoints. However, for SGRB050724 we could not find any of the observed line ratios generally used to model the host galaxy. For SGRB050709 we calculate the continuum SED by model modb4 (Table 3) at the nebula. Savaglio et al data for SGRB050709 are reproduced by a stellar background bb at $T_{bb}=3000 \text{ K}$ in Fig. 2. Proceeding as for NGC4993 (Sect. 3.1) we combined $H\beta_{calc}$ (Table 3) with $H\beta_{obs}$ presented by Berger (2009, table 2). Adopting $ff=0.01$ we calculated f_s and accordingly we shifted the calculated continuum in Fig. 2. Hopefully future data will confirm the modelling. The distance of the emitting nebula from the photoionizing source r results 144 pc .

Table 2. Modelling Berger (2009) SBLG spectra

GRB	z	[OII] 3727	H β 4865	[OIII] 5007+	H α 6563	[NII] 6548+	ref
061006 ¹	0.4377	4.1	0.9	1.5	-	-	Berger (2009)
061006 ²		4.24	1	1.89	-	-	
modb1		4.5	1	1.86	-	-	
061210 ¹	0.4095	22.	7.6	10.5	11.	2.4	Berger (2009)
061210 ³		1.71	1	1.6	3	0.15	
modb2		1.77	1	1.57	2.98	0.15	
070724 ¹	0.4571	37.	15.	17.	-	-	Berger (2009)
070724 ²		2.47	1	1.13	-	-	
modb3		2.54	1	1.18	-	-	
050709 ¹	0.1606	-	6.6	26.	26.	1.8	Fox et al (2005)
050709 ³		-	1	3.7	3.	0.29	
modb4		(1.69)	1	3.78	3	0.29	

¹ line flux in 10^{-17} erg cm⁻² s⁻¹ observed at Earth; ² line ratios to H β ; ³ corrected line ratios to H β

Table 3. Models for Berger (2009) SBLG spectra

mod	V_s km s ⁻¹	n_0 cm ⁻³	D 10 ¹⁸ cm	12+log(N/H)	12+log(O/H)	T_* 10 ⁴ K	U -	H β 1	12+log(O/H)(Berger)
modb1	100	100	0.8	7.	8.82	5.7	0.005	0.006	8.63
modb2	100	300	2.8	6.9	8.8	4.3	0.03	0.167	8.82
modb3	120	250	3.	-	8.81	4.9	0.013	0.072	8.88
modb4	120	250	3.	7.25	8.81	4.8	0.06	0.19	8.50

¹ in erg cm⁻² s⁻¹ calculated at the nebula;

Table 4. Modelling Perley et al (2012) short GRB100206A host spectra at $z=0.4068$

	[OII] 3727	H β 4865	[OIII] 5007+	H α 6563	[NII] 6548+	[SII] 6716	[SII] 6731
subtr ¹	19.6	21.8	6.8	112.8	58.8	20.4	13.6
F/H β	0.9	1	0.31	5.17	2.7	0.93	0.62
corr	1.34	1	0.23	3.	1.58	0.53	0.35
modp1	1.6	1	0.23	3.	1.54	0.43	0.35
North (subtr) ¹	7.91	9.59	1.22	33.41	16.98	4.44	4.0
F/H β	0.82	1	0.127	3.48	1.77	0.46	0.42
modp2	0.82	1	0.127	3.12	1.6	0.4	0.42
Center (subtr) ¹	5.69	7.57	3.5	60.55	33.9	3.33	3.24
F/H β	0.75	1	0.46	8.	4.47	0.44	0.43
corr	1.57	1	0.27	3.	1.67	0.15	0.149
modp3	1.64	1	0.28	3.2	1.4	0.14	0.14
South (subtr) ¹	4.02	3.61	1.68	17.7	10.54	3.06	4.94
F/H β	1.11	1	0.465	4.9	2.92	0.85	1.37
corr	1.6	1	0.36	3.	1.8	0.5	0.81
modp4	1.57	1	0.367	3.2	1.8	0.51	0.61

¹ in 10^{-17} erg cm⁻² s⁻¹

Table 5. Models for Perley et al (2012) GRB100206A spectra

	V_s km s ⁻¹	n_0 cm ⁻³	D 10 ¹⁸ cm	12+log(N/H)	12+log(O/H)	12+log(S/H)	T_* 10 ⁴ K	U 0.001	H β 1
modp1	100	120	4.9	8.04	8.78	6.48	4.4	0.9	0.003
modp2	100	250	3.3	8.25	8.82	6.95	3.6	0.6	0.025
modp3	100	200	3.3	8.04	8.82	6.40	4.6	0.6	0.0098
modp4	120	200	1.9	8.15	8.82	7.11	4.	0.6	0.0092

¹ in erg cm⁻² s⁻¹ calculated at the nebula

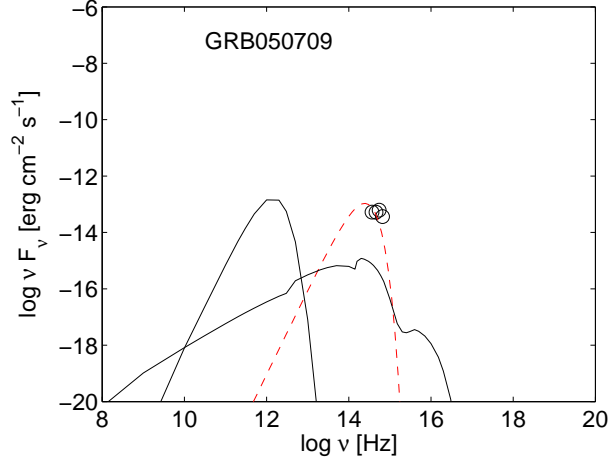


Figure 2. The SED of SGRB050709 host from the Savaglio et al sample. Open circles : the data; black solid lines : model modb4 (Table 3); dashed line : bb flux corresponding to $T_{bb}=3000\text{K}$.

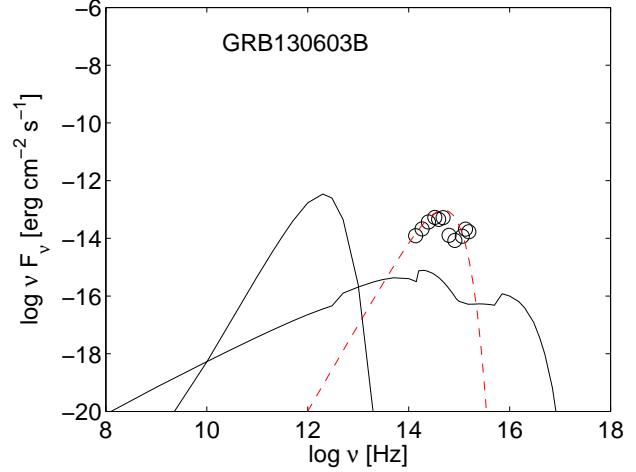


Figure 4. The SED of GRB130603B host from the de Ugarte Postigo et al sample. Open circles : the data; black solid lines : model MS5 (Table 6); dashed line : bb flux corresponding to $T_{bb}=6000\text{K}$.

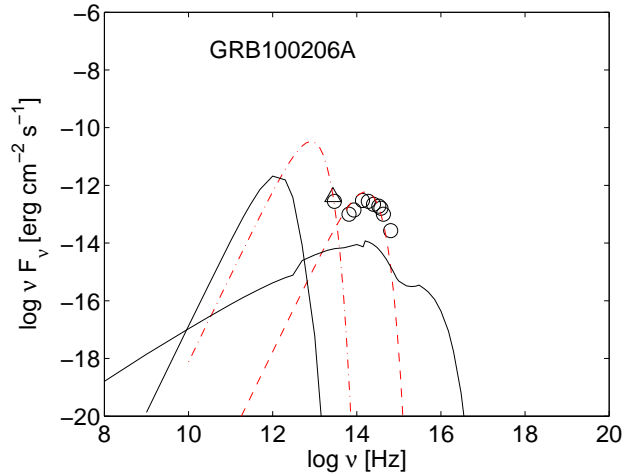


Figure 3. The SED of SGRB100206A host from the Perley et al sample. Open circles : the data; black solid lines : model modp1 (Table 5); dashed line : bb flux corresponding to $T_{bb}=2000\text{K}$; dash-dotted line : bb flux corresponding to $T_{bb}=100\text{K}$.

3.3 Spectra of short GRB100206A host by Perley et al (2012)

Perley et al (2012) presented data from Swift for GRB100206A (Table 4) a disk galaxy at $z=0.4068$ rapidly forming stars. The galaxy is red, obscured and the interpretation of the spectra reported by Perley et al leads to a high metallicity ($12+\log(\text{O}/\text{H})=9.2$). They also explain the SED by a substantial stellar mass of older stars although the IR luminosity ($4 \times 10^{11} L_{\odot}$) could indicate young star formation. Perley et al show a single spectrum and the spectra observed in different locations with the particular aim to determine the metallicity (in term of O/H). We present in Table 5 the physical conditions calculated by the detailed modelling of the spectra presented by Perley et al (2012) in their tables 2 and 3. Unfortunately the lines are few, nevertheless they are the minimum required to constrain the models. Our re-

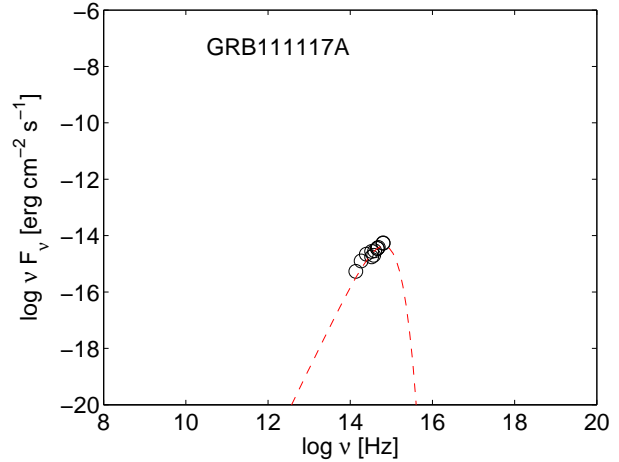
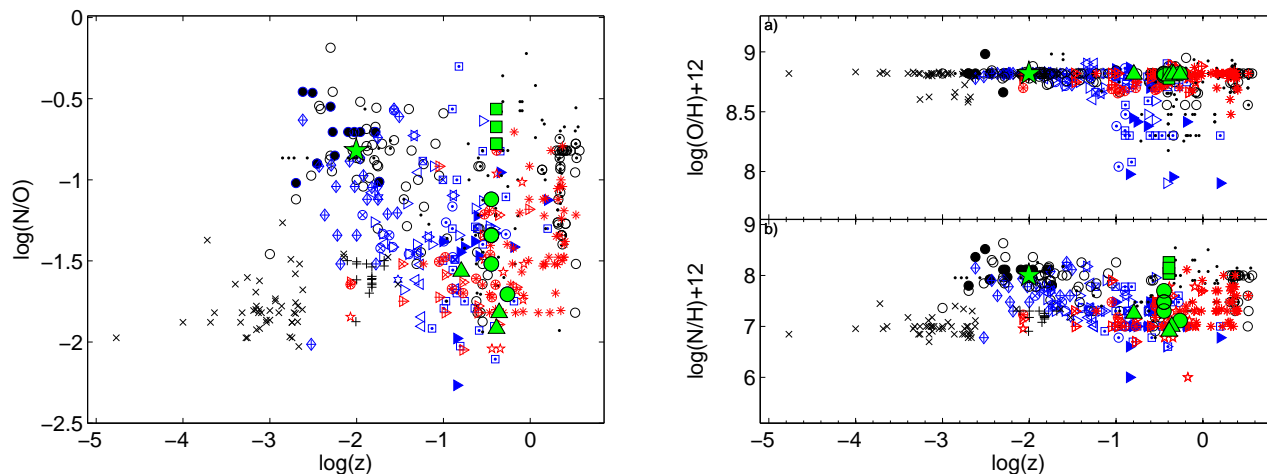


Figure 5. The SED of GRB111117A host from Selsing et al. Open circles : the data; dashed line : bb flux corresponding to $T_{bb}=8000\text{K}$.

sults show relatively high preshock densities in the emitting clouds which are more extended than those in LGRB hosts (Contini 2017a). We find solar O/H ($12+\log(\text{O}/\text{H})=8.82$) in nearly all the observed positions, while N/H are higher than solar by a small factor (<2), but higher by a factor of ~ 10 than for the SGRB hosts in the Berger sample. The N/O ratios are the highest ever calculated for SGRB, even higher than those calculated for the de Ugarte Postigo et al (2014) GRB spectra and those calculated for long GRB at the same redshift. The stellar background contribution to the SED corresponds to $T_{bb}=2000\text{K}$. The calculated SED is shown in Fig. 3.

Table 6. Models for SGRB 130603B at $z=0.356$ and SGRB 051221a at $z=0.546$ host galaxy spectra

	OT site ¹	mS1	OT site ²	mS2	core ²	mS3	arm ²	mS4	obs ³	mS5	051221a ⁴	mS6
[OII]3727+	4.47	4.5	3.4	3.6	3.55	3.7	4.3	4.3	3.05	3.2	7.8	7.5
H γ	-	0.46	0.89	0.49	0.49	0.46	[0.5]	0.46	-	0.46	0.46	0.46
H β	1	1	1	1	1	1	1	1	1	1	1	1
[OIII]5007+	0.87	0.9	0.76	0.8	0.75	0.8	0.85	0.85	0.77	0.7	5.17	5.15
H α	3.	3.	3.	2.96	3.	2.96	3.	3.	3.	3.	-	3.
[NII]6585	0.7	0.76	0.57	0.56	0.85	0.85	1.8	1.8	0.78	0.8	-	-
[SII]6717	0.66	0.7	1.19	1.1	0.63	0.66	0.27	0.5	-	-	-	-
[SII]6731	0.33	0.6	0.56	0.97	0.5	0.59	0.5	0.45	-	-	-	-
V _s (km s ⁻¹)	-	140	-	150	-	150	-	140	-	120	-	150
n ₀ (cm ⁻³)	-	120	-	130	-	130	-	120	-	100	-	100
B ₀ (10 ⁻⁴ G)	-	3	-	3	-	3	-	3	-	2	-	1
D ⁵	-	5.3	-	1	-	1	-	1	-	3	-	0.2
12+log(O/H)	-	8.82	-	8.8	-	8.8	-	8.82	-	8.81	-	8.82
12+log(N/H)	-	7.3	-	7.3	-	7.48	-	7.8	-	7.48	-	7.11
12+log(S/H)	-	6.6	-	7.0	-	6.78	-	6.48	-	6.48	-	6.48
T _* (10 ⁴ K)	-	3.6	-	3.5	-	3.5	-	3.6	-	3.8	-	8.3
U	-	0.014	-	0.01	-	0.01	-	0.014	-	0.007	-	0.007
H β ⁶	-	0.014	-	0.016	-	0.016	-	0.03	-	0.014	-	0.007
12+log(O/H) ⁷	-	7.94-8.98	-	8.16-8.88	-	8.17-8.87	-	8.26-8.77	-	8.5	-	8.7

¹de Ugarte Postigo et al (2014)(X-shooter); ²de Ugarte Postigo et al (2014)(FORS);³ Cucchiara et al (2013)(DEIMOS); ⁴ Soderberg et al (2006)(Gemini-N GMOS); ⁵ in 10¹⁸ cm; ⁶ in erg cm⁻² s⁻¹; ⁷ evaluated by the observers adopting the strong line method.

Figure 6. Left: distribution of N/O calculated by detailed modelling for SGRB hosts as function of the redshift (large circles : from the spectra observed by de Ugarte Postigo et al; large squares : from Perley et al; large triangles : from Berger; large star: NGC4993). The results obtained in the present paper are superposed on those calculated for SN host galaxies (small triangles, filled diamonds, points inside a square), long GRB hosts (asterisks), short GRB hosts (stars), SB (dots), AGN (open circles) and LINERs (filled circles) both local and at higher z ; plus and cross : HII region galaxies nearby and local, respectively. Right : the same for O/H and N/H relative abundances. Symbols as in the left diagram; References are given by Contini (2017a, table 9).

3.4 SGRB130603B (de Ugarte Postigo 2014) and SGRB051221a (Soderberg et al 2006)

We report in the following the modelling of SGRB130603B and SGRB051221a line ratios by Contini (2016). We present in Fig. 4 the modelling of the SED. The spectra by FORS2 and X-shooter at VLT and ACAM at WHT were observed by de Ugarte Postigo et al (2014). They suggested that SGRB derive from the merger of compact objects, in particular SGRB 130603B, on the basis of the detection of "kilonova"-like signature associated with Swift. The host galaxy is a perturbed spiral due to interaction with another

galaxy (de Ugarte Postigo et al). In the spectrum taken by X-shooter the afterglow dominates the continuum, but the lines are emitted from the host therefore they are used for modelling. FORS spectra show the core, the arm and the opposite side of the galaxy. The GRB is located in the outskirts of the galaxy in a tidally disrupted arm at ~ 5.4 kpc from the brightest point of the host. The host was covered by two slit positions along the major axis and two spectra were taken at different times plus a X-shooter spectrum covering the afterglow position. The results of modelling the X-shooter and FORS reddening corrected spectra observed by de Ugarte Postigo et al (see Contini 2016, table 12) are reported in

Table 6, neglecting the GTC spectra because they do not include the $H\alpha$ line. The spectrum observed by Cucchiara et al (2013) for SGRB 130603B is also shown for comparison. Most of the spectra presented by SGRB surveys (e.g. Fong et al 2013) do not contain enough lines to constrain the models. To best reproduce all the line ratios presented in Table 6 S/H lower than solar ($(S/H)_{\odot} = 1.6 \times 10^{-5}$, Grevesse & Sauval 1998) by factors ≥ 2 were adopted. S/H in FORS (OT site) is near solar. The cloud geometrical thickness results relatively large ($D=1.8$ pc) from the modelling of the X-shooter (OT site) results. $D=0.3$ pc is used to fit the FORS spectra, showing a larger cloud fragmentation. The spectrum reported by Cucchiara et al (2013) is reproduced by model (mS5) similar to those used to fit the spectra observed by de Ugarte Postigo et al. The SB temperatures and ionization parameters which result from modelling the host spectra are relatively low ($T_* \sim 3.5 \times 10^4$ K and $U \sim 0.01$).

The spectrum observed by Soderberg et al (2006) for SGRB051221a at $z=0.546$ and the relative model mS6 are reported from Contini (2016, table 12, last two columns) in Table 6. The line ratios were reddening corrected adopting $H\gamma/H\beta=0.46$. The best fitting model shows $12+\log(O/H)=8.8$, in agreement with Soderberg et al who obtained 8.7 by the R32 method (upper branch). We have found $T_* = 8.2 \times 10^4$ K and $U=0.007$. T_* is higher than for SGRB130603B, where $T_* \sim 3.5 \times 10^4$ K. U , however, is similar. Low ionization parameters (i.e. the number of photons reaching the nebula per number of electrons at the nebula) roughly indicate that the host observed positions are far from the star-forming region or that the photon flux is prevented from reaching the nebula. The hosts show $N/H \leq 0.5$ solar and O/H solar.

The continuum SED of SGRB130603B (de Ugarte Postigo 2014) appears in Fig. 4. The star background contribution to SGRB130603B corresponds to $T_* = 6000$ K. For SGRB051221a the photometric data are too few to be used for modelling the SED.

3.5 GRB111117A host SED (Selsing et al 2017)

Selsing et al (2017) presented spectroscopy and photometry data of GRB 111117A host galaxy with an estimated redshift of $z=2.211$. The galaxy is actively forming stars. At $z=2.211$ GRB111117A is the most distant high-confidence SGRB detected to date. Spectroscopic observations used VLT/X-shooter (Vernet et al 2011) at four separate epochs. The burst was observed 38 hours after the BAT trigger. Selsing et al determined the redshift value from the simultaneous detection of emission lines belonging to $Ly\alpha$, [OII]3727, [OIII]5007 and $H\alpha$, but $H\beta$ was detected at low significance. They used $F_{H\alpha} = 4.1 \times 10^{-17}$ erg cm $^{-2}$ s $^{-1}$ to calculate the $SFR=18 \pm 3 M_{\odot}$ yr $^{-1}$. No dust was deduced from the $Ly\alpha$, so the spectra were not reddening corrected. Selsing et al photometric data appear in Fig. 5. They are reproduced by a bb flux corresponding to $T_{bb}=8000$ K, in agreement with Margutti et al (2012) who reported that GRB111117A has a young age and vigorous star formation.

4 CONCLUDING REMARKS

In this work we have presented the analysis of line and continuum spectra of a few SGRB host galaxies by exploiting the spectroscopic and photometric data available in the literature. For some objects included in our sample the spectra show the [OIII]/ $H\beta$ and [NII]/ $H\alpha$ line ratios. These diagnostics (e.g. Baldwin et al 1981, Kewley et al 2001, etc) are generally used to recognise the type of flux which photoionizes the GRB host gas (a bb for SBs, HII regions or a power-law for AGNs). Even if the literature data are sometimes poor and have not always allowed us to constrain the analysis results, we have nevertheless managed by the detailed modelling of other line ratios (e.g. [OII]3727+/ $H\beta$, [SII]6717/[SII]6731, etc) to obtain a more complete picture of the gas physical conditions (i.e. shock velocity, preshock density, geometrical thickness of the emitting clouds, flux intensity from the AGN or from the SB, SB effective temperature and ionization parameter) and chemical abundances.

We have investigated in particular NGC4993, the host galaxy of GW170817. We confirm that an AGN, such as a LLAGN or a LINER, must be the source of gas photoionization. NGC4993 was formerly identified as a LLAGN on the basis of the BTP diagrams. Shock velocities (~ 100 km s $^{-1}$) and preshock densities (~ 300 cm $^{-3}$), constrained by the simultaneous and consistent fit of the line ratios and of the SED, are similar to those found in the AGN NLR. By modelling the continuum SED we have also found that the contribution of an old stellar population background with $T_{bb}=4000$ K is very high relative to the Bremsstrahlung in the near IR range and higher by a factor > 100 than for local AGN and SB galaxies. O/H and N/H relative abundances are solar.

On the basis of the results obtained for NGC 4993 and for LGRB hosts (Contini 2018) and for different types of local galaxies (AGN SB, etc e.g. Contini & Contini 2007) we suggest that Bremsstrahlung from the clouds which emit the line spectra could also be the main contributor to the continuum in the radio, optical, UV and soft X-ray range of SGRB hosts, while the stellar background bb radiation in the IR-optical domain is constrained by the photometry observations in the IR. Moreover, dust reprocessed radiation in the IR range (consistently calculated with the gas Bremsstrahlung) and the flux from the photoionising source in the X-ray are also considered. The results calculated for the SGRB hosts are summarized in Table 7.

In Fig. 6 diagrams we have added the N/O ratios calculated for the SGRB hosts as a function of the redshift to those presented for LGRB hosts, SN hosts of many types, HII regions, AGN, LINER and SB galaxies (Contini 2016). The right diagrams show the results for O/H and N/H as a function of z . It is evident that O/H is about constant at the solar value, while N/O covers a large range of values determined by the N/H ratios ($6.8 \leq \log(N/H) + 12 \leq 8.25$) throughout a very small redshift range centered around $z \sim 0.4$. N/O abundance ratios calculated in GRB100206B along different positions – observed by Perley et al. – reach the maximum values calculated for LGRB hosts at higher redshifts. At present, only few data at other z are available. NGC4993 is located within the AGN and LINER region at a redshift close to local. Compared with LGRB and SGRB hosts (Contini 2016), the most significant characteristic of NGC4993 is

Table 7. Results of detailed modelling calculations

SGRB	V_s km s ⁻¹	n_0 cm ⁻³	D pc	12+log(N/H) -	12+log(O/H) -	T_* 10 ⁴ K	U -	log(F) 1	H β 2	T_{bb} K	z
NGC4993	100	300	0.3	8.	8.82	-	-	9.55	0.05	4000	0.009873
050709	120	250	1.	7.25	8.81	4.8	0.06	-	0.19	3000	0.167
051221a	150	100	0.07	7.11	8.82	8.3	0.007	-	0.007	-	0.546
061006	100	100	0.27	7.0	8.82	5.7	0.05	-	0.006	-	0.4377
061210	100	300	0.93	6.9	8.80	4.3	0.03	-	0.167	-	0.4095
070724	120	250	1.	7.25	8.81	4.9	0.013	-	0.072	-	0.4571
100206A	100	120	1.7	8.04	8.78	4.4	0.9	-	0.003	2000	0.4068
100206A N	100	250	1.1	8.25	8.82	3.6	0.6	-	0.025	-	-
100206A C	100	200	1.1	8.04	8.82	4.6	0.6	-	0.0098	-	-
100206A S	120	200	0.7	8.15	8.82	4.	0.6	-	0.0092	-	-
130603B OT ³	140	120	1.8	7.30	8.82	3.6	0.014	-	0.014	6000	0.356
130603B OT ⁴	150	130	0.3	7.30	8.80	3.5	0.01	-	0.016	-	-
130603B core	150	130	0.3	7.48	8.80	3.5	0.01	-	0.016	-	-
130603B arm	140	120	0.3	7.7	8.82	3.6	0.014	-	0.03	-	-
130603B ⁵	120	100	1.	7.47	8.813	3.8	0.007	-	0.014	-	-

¹F is in photon cm⁻² s⁻¹ eV⁻¹ at the Lyman limit; ² in erg cm⁻² s⁻¹ calculated at the nebula; ³ X- shooter; ⁴ FORS; ⁵DEIMOS

the presence of an AGN source. Actually, NGC4993 is the only SGRB host lying among AGN, LINERs and LLAGN at low z (see Fig. 6). Whether this is an isolated case it is not yet known. However, the high evolution age and/or a different nuclear development related to the primary nitrogen should be considered. More data are needed.

Most of the other SGRB are located at the confluence (at z close to 0.4) of the N/O decreasing slope with decreasing z of GRB hosts and of the increasing N/O slope with decreasing z of SN hosts at lower z (Fig. 6). Intermediate-mass stars between 4 and 8 M_\odot dominate nitrogen production, which is primary at low metallicities, but when 12+log(O/H) exceeds 8.3, secondary N production occurs, increasing at a faster rate than O (Henry et al 2000). The data are few, but it seems that N/O ratios in the present SGRB sample follow a different trend.

ACKNOWLEDGEMENTS

I am very grateful to the referee for critical suggestions which substantially improved the presentation of the paper.

REFERENCES

- Baldwin, J., Phillips, M., Terlevich, R. 1981, PASP, 93, 5
 Barthelmy, S.D. et al 2005, Nature, 438, 994
 Bell, A.R. 1977, MNRAS, 179, 573
 Berger, E. 2014, ARA&A, 52, 43
 Berger, E. 2013, ApJ, 765, 121
 Berger, E. 2009, ApJ, 690, 231
 Berger, E. et al 2005, Nature, 438, 988
 Blanchard, P.K. et al 2017, ApJL, 848, L22
 Bloom, J.S., Kulkarni, S.R., Djorgavski, S.G. 2002, AJ, 123, 1111
 Contini, M. 2018, submitted
 Contini, M. 2017a, MNRAS, 469, 3125
 Contini, M. 2017b, MNRAS, 466, 2787
 Contini, M. 2016, MNRAS, 460, 3232
 Contini, M. 2004, MNRAS, 675, 683
 Contini, M. & Contini, T. 2007, AN, 328, 953
 Contini, M. & Viegas, S.M. 2001a ApJS, 137, 75
 Contini, M. & Viegas, S.M. 2001b ApJS, 132, 211
 Contini, M. & Aldrovandi, S.M.V. 1983 A&A, 127, 15
 Contini, M., Prieto, M.A. & Viegas, S.M. 1998a, ApJ, 505, 621
 Contini, M., Prieto, M.A. & Viegas, S.M. 1998b, ApJ, 492, 511
 Cox, D.P. 1972, ApJ, 178, 143
 Cucchiara, A. et al 2013, ApJ, 777, 94
 D'Avanzo, P. 2015, JHEAp, 7, 73
 de Ugarte Postigo, A. et al. 2014, A&A, 563, 62
 De Vaucouleurs, G., De Vaucouleurs, A., Corwin Jr., H.J., Buta, R.J., Paturel, G., Fouque, P. 1991 Third reference catalogue of bright galaxies, RC3.9
 Draine, B.T. & Lee, M.M. 1994, ApJ, 285, 89
 Eichler, D., Livio, M., Piran, T., Schramm, D.N. 1989, Nature, 340, 126
 Ferland G. et al 1995, The Analysis of Emission Lines: A Meeting in Honor of the 70th Birthdays of D. E. Osterbrock & M. J. Seaton, proceedings of the Space Telescope Science Institute Symposium, held in Baltimore, Maryland May 16–18, 1994, Eds.: Robert Williams and Mario Livio, Cambridge University Press, p. 83, ArXiv:160308902
 Fong, W. et al 2013, ApJ 769, 56
 Fox, D.B., Frail, D.A., Hurley, K.C. et al 2005, Nature, 437, 845
 Fruchter, , A.S et al 2006, Nature, 441, 463
 Gehrels, N., White, N., Barthelmy, S. et al 2004, ApJ, 611, 1005
 Grevesse, N., Sauval, A.J. 1998 SSRv, 85, 161
 Haggard, D. et al 2017, ApJ, 848, L25
 Henry, R.B.C., Edmund, M.G. & Köppen, J. 2000, ApJ, 541, 660
 Hunt, L.K. et al 2014, A&A, 565, A112
 Kann, D.A. 2011, ApJ, 734, 96
 Kauffmann, G. et al 2003, MNRAS, 346, 1055
 Kennicutt, R.C. 1998, ARA&A, 36, 189

- Kewley, L., Dopita, M.M., Sutherland, R., Heisler, C.,
Trevena, J. 2001, ApJ, 556, 121
- Kouvelioutou, C et al 1993, ApJL, 413, L101
- Lambert, A. & Valentijn, E.A. 1989, The Surface Photometry Catalogue of the ESO-Uppsala, 1989, Garching bei Munchen:ESO
- Levan, A.J. et al. 2017 ApJL (in press. arXiv:1710.05444)
- Margutti, R., Berger, E. , Fong, W. et al 2012, ApJ, 756, 63
- Maraston, C. 2005, MNRAS, 362, 799
- Niino, Y. et al 2016 Publ. Astron. Soc. Japan, arXiv:1606.01983
- Osterbrock, D.E. 1974, in Astrophysics of Gaseous Nebulae, W.H Freeman and Co., San Francisco
- Palmese, A. et al 2017, arXiv:1710.06748
- Pan, Y.-C. et al 2017, ApJ, 848, L30
- Perley, D.A. et al. 2012, ApJ, 758, 122
- Rigby, J.R.& Rieke, G.H. 2004, ApJ, 606,237
- Rosswog, S., Ramirez-Ruiz, E., Davies, Melvyn B, 2003, MNRAS, 345, 1077
- Savaglio, S., Glazerbrook, K., Le Borgne, D. 2009, ApJ, 691, 182
- Selsing, J. et al 2017 arXiv:1707.01452
- Soderberg, A.M. et al 2006, ApJ, 650, 261
- Vernet, J. et al. 2011, A&A, 536, A105
- Viegas, S.M. & Contini, M. 1994, ApJ, 428, 113
- Villar, V.A. et al 2017, arXiv:1710.11576
- Williams, R.E. 1967, ApJ, 147, 556
- Wu, Q., Feng, J., Fan, X. 2017, arXiv:1710.09590